Supplementary Information

Metal organic framework-induced Mesoporous Carbon Nanofibers as Ultrastable Na Metal Anode Host
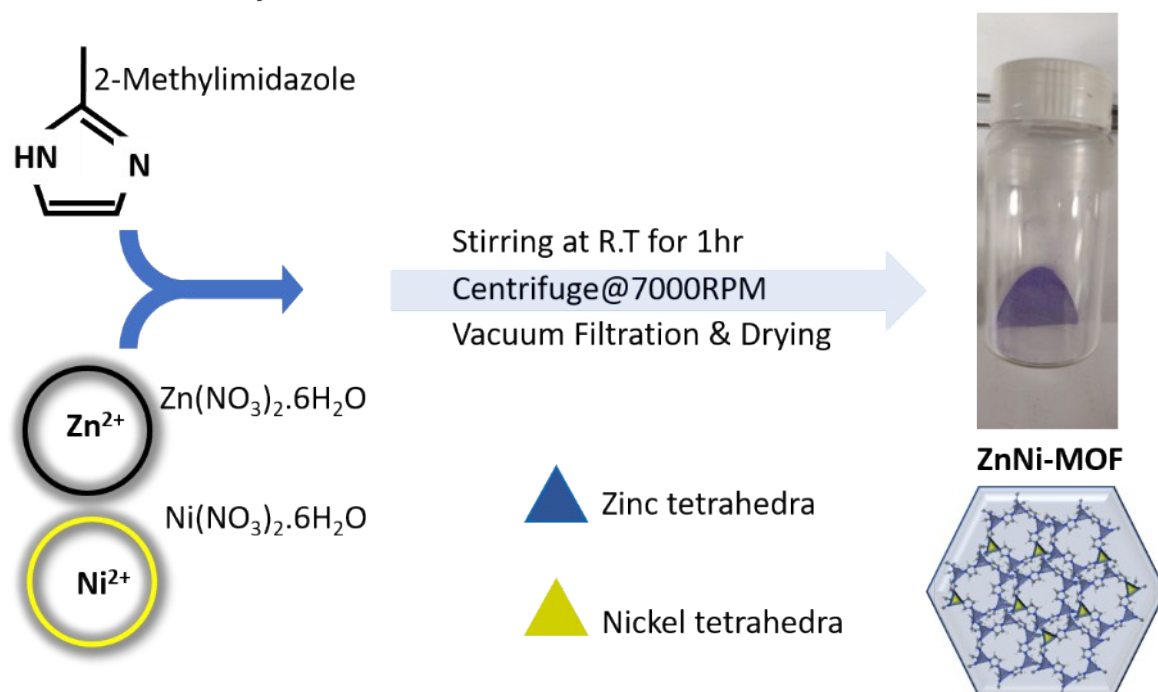

Fig. S1. A schematic representation of bimetallic MOF synthesis. Purple and yellow triangles represent Zinc and Ni atomic clusters, respectively, while pentagonal ring structure is associated with imidazole ligand.
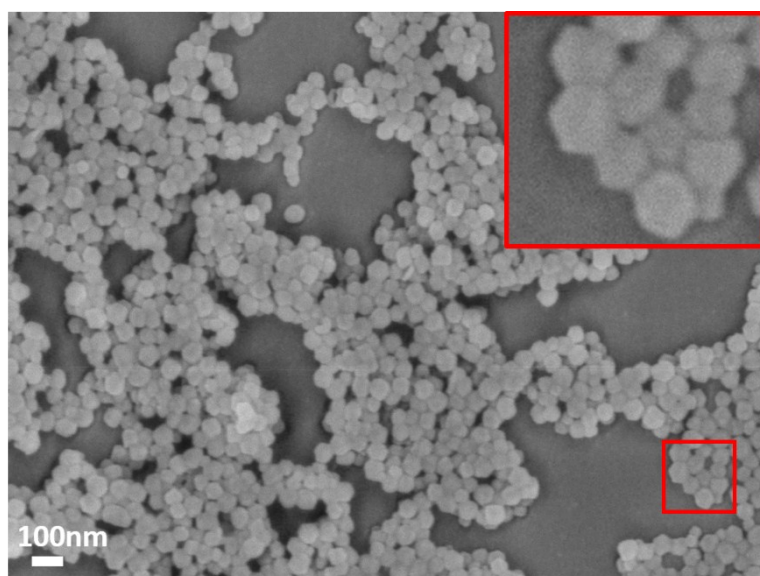

Fig. S2. SEM micrograph of synthesized MOF nanoparticles with a truncated dodecahedral geometry and ~50 nm in diameter. Inset shows a magnified view of nanoparticles.
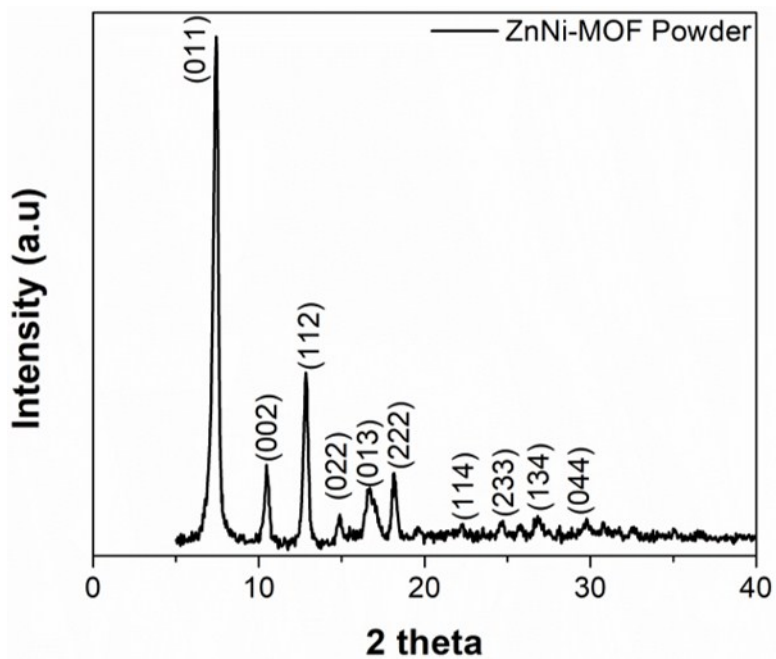
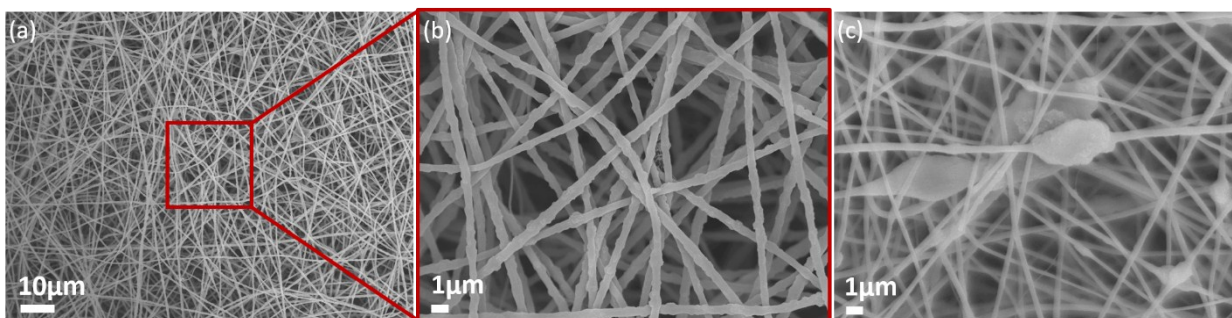Fig. S3. XRD spectrum of MOF nanoparticles showing characteristic peaks

Fig. S4. SEM micrographs of MCNFs with (a-b) an optimized MOF concentration for uniform dispersion and (c) an excessive MOF concentration causing agglomeration.
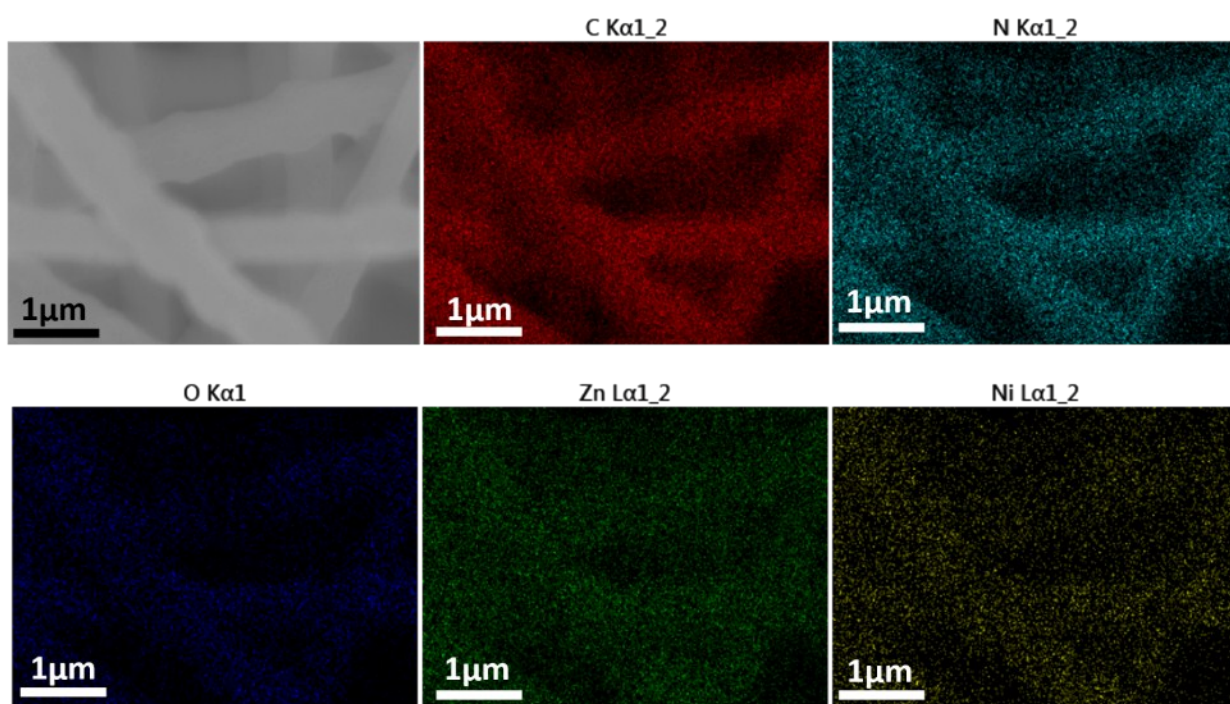
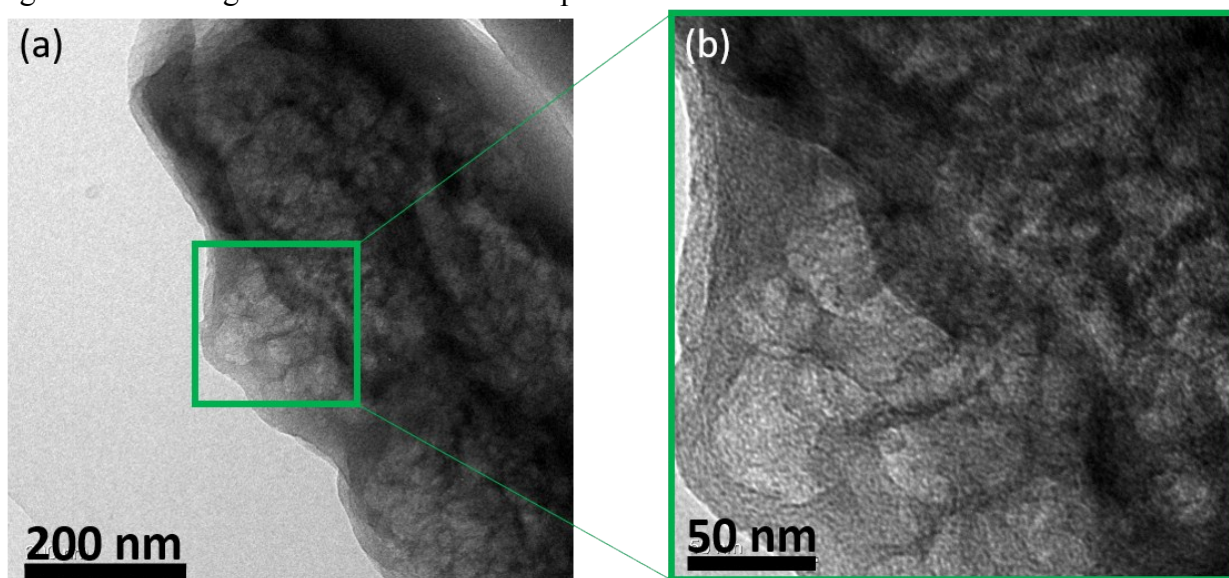Fig. S5. SEM image and EDX elemental maps of PCNF-800.

Fig. S6. HRTEM images of PCNFs showing mesopores of size below 50 nm upon decomposition of MOF and contraction by carbonization.
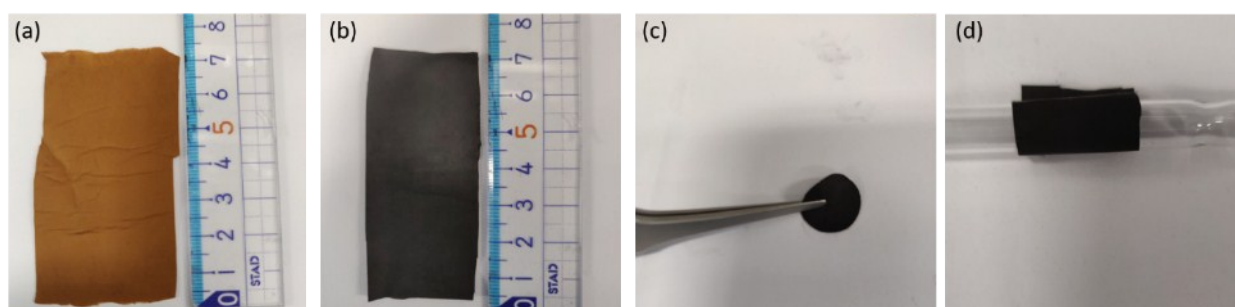

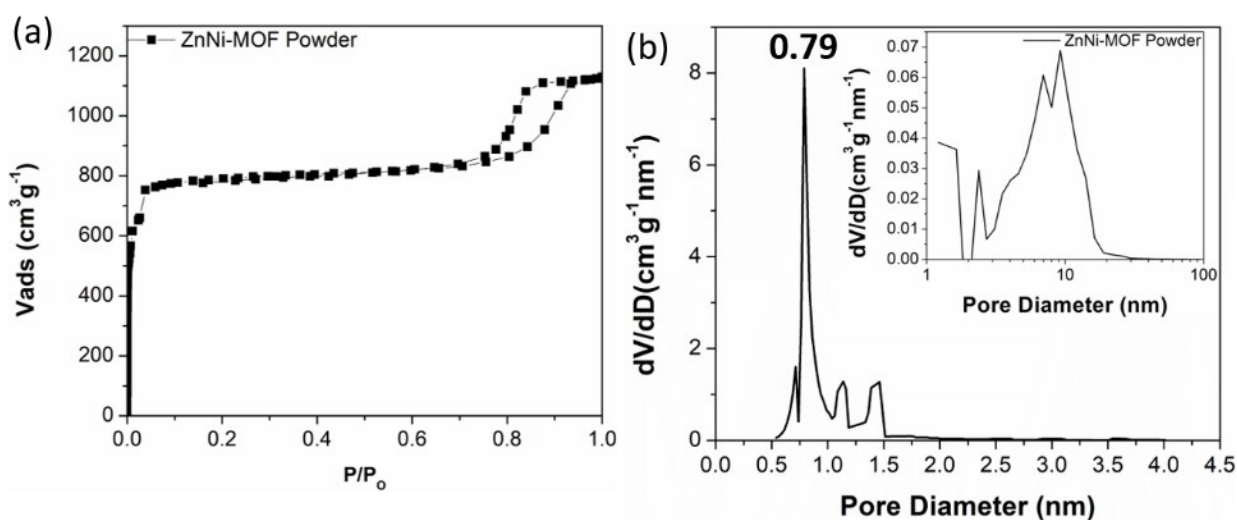Fig. S7. Digital images of PCNF (a) before (b-d) after carbonization.

Fig. S8. (a) Nitrogen adsorption/desorption isotherm; and (b) Pore size distribution of MOF nanoparticles with HK micropores: BJH pore size distribution in inset.
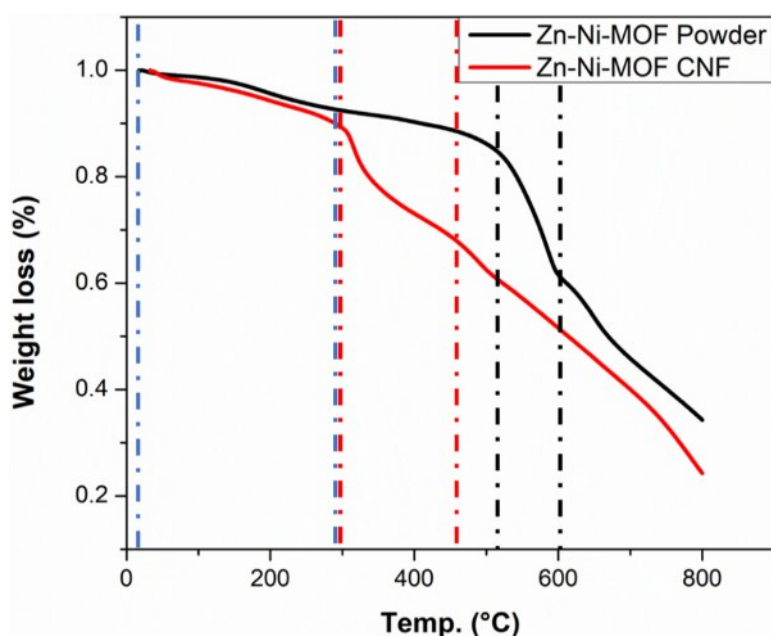
Fig. S9. TGA curves of bimetallic MOF powder and MOF CNF obtained in an Ar atmosphere.

The pores inevitably generated a large number of defects in the carbon network, which were quantified via the Raman spectroscopic analysis (Fig. S10). The peaks located at 1350 cm^{-1} and 1595 cm^{-1} can be attributed to the disordered (D) and ordered, or graphitic (G), carbon, respectively. [S1] As expected, the PCNF films carbonized at a low temperature of 700°C exhibited the highest I_D/I_G ratio of 1.64 due to the presence of a large quantity of disordered structures. Increasing the carbonization temperature led to a steady decrease in I_D/I_G ratio. The pristine CNF films exhibited much sharper G peaks corroborating their more ordered structure than the mesoporous PCNFs. Nevertheless, both

4

CNFs and PCNFs possessed predominantly amorphous structures as verified by the XRD analysis (Fig. S11).
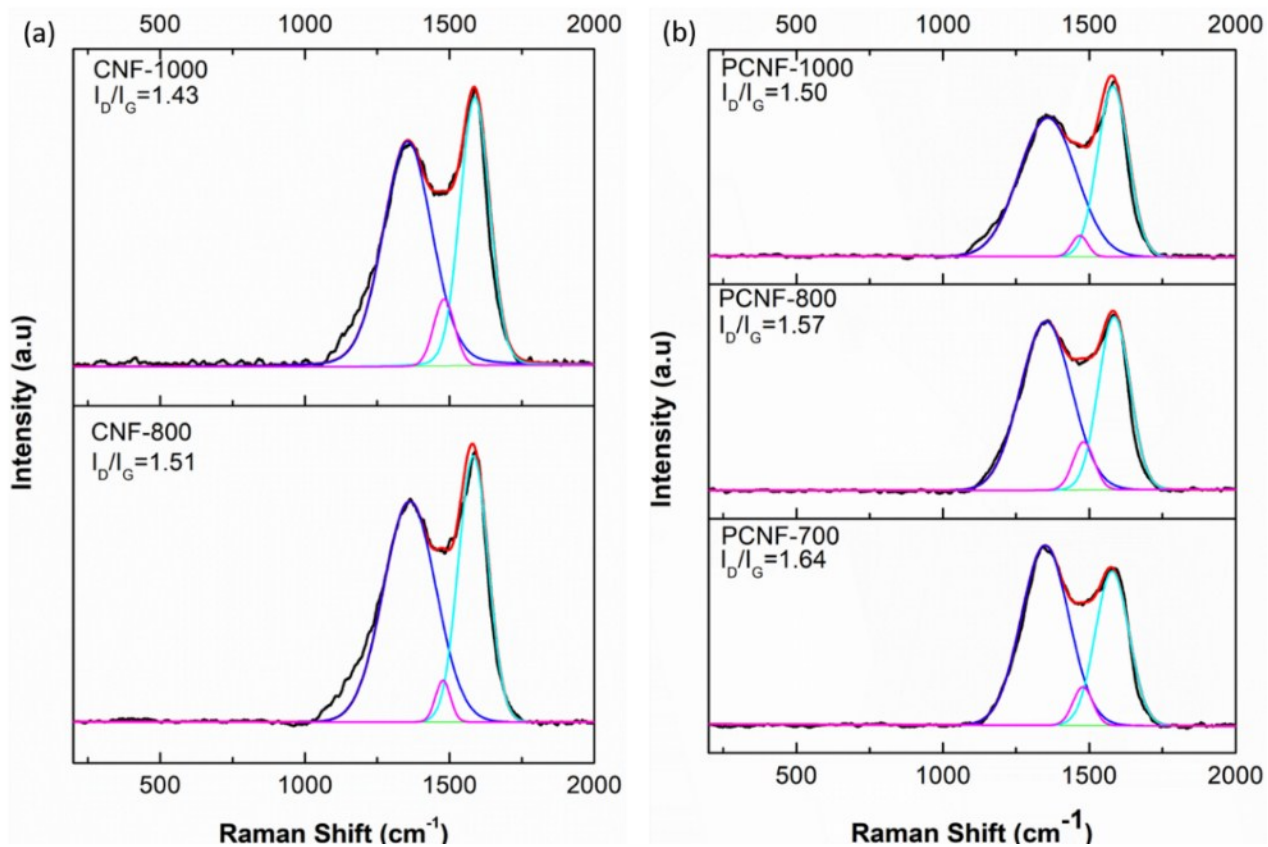
Fig. S10. Raman spectra of (a) CNFs and (b) PCNFs taken at different carbonization temperatures.
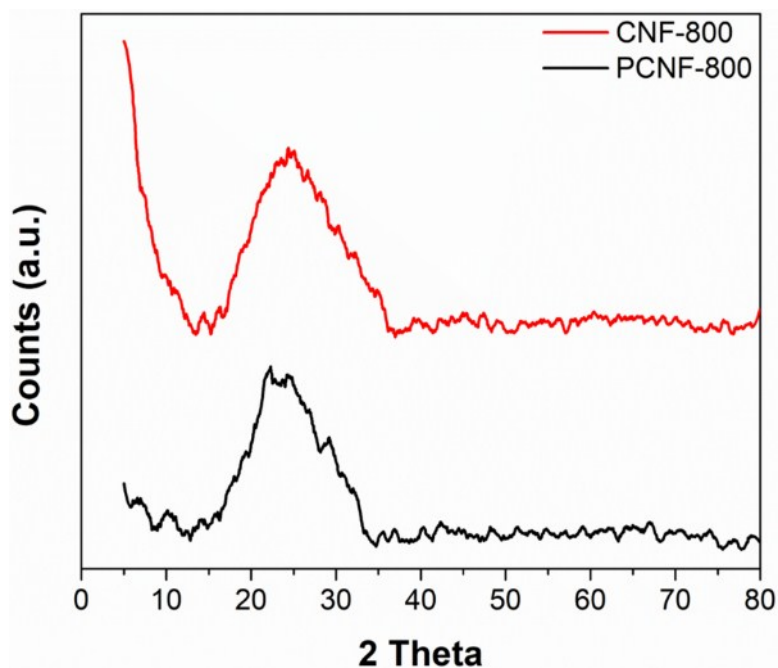
Fig. S11. XRD spectra of CNF and PCNF carbonized at 800°C.
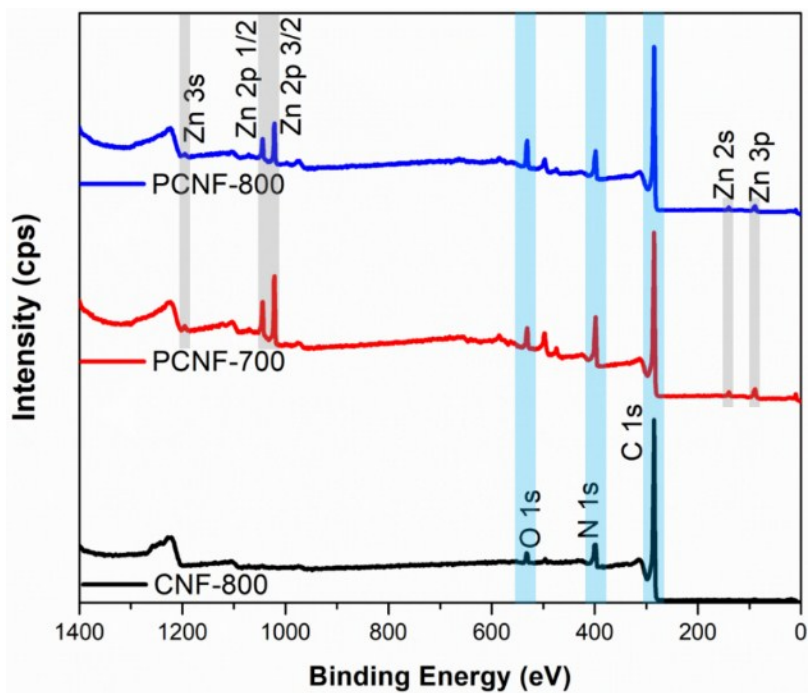
Fig. S12. XPS survey spectra of CNF and PCNF.
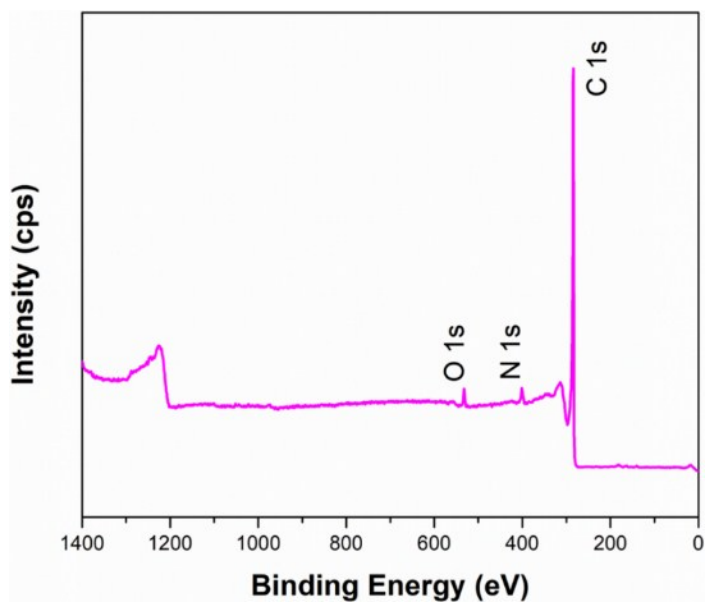
Fig. S13. XPS survey spectrum of PCNF-1000.
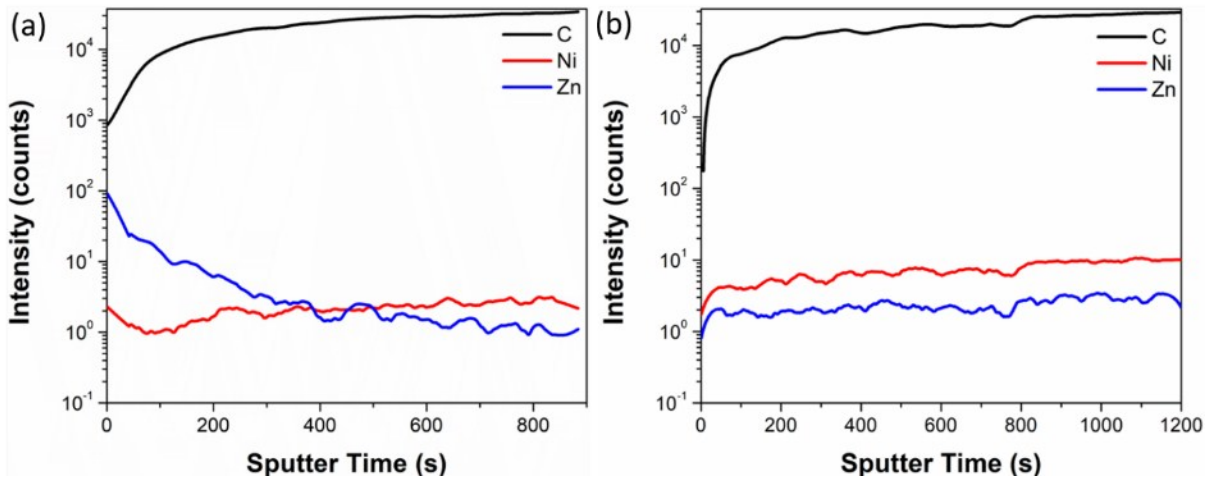
Fig. S14. TOF-SIMS profiles of (a) PCNF-800 and (b) PCNF-1000.
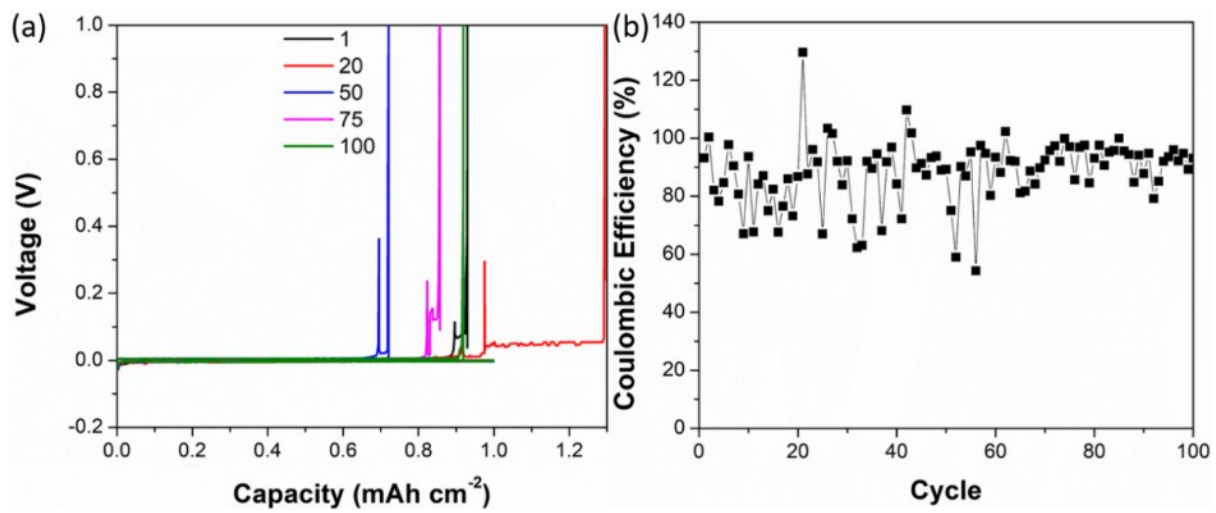
Fig. S15. (a) Half-cell voltage profiles; and (b) Coulombic efficiencies of Cu foil current collector.
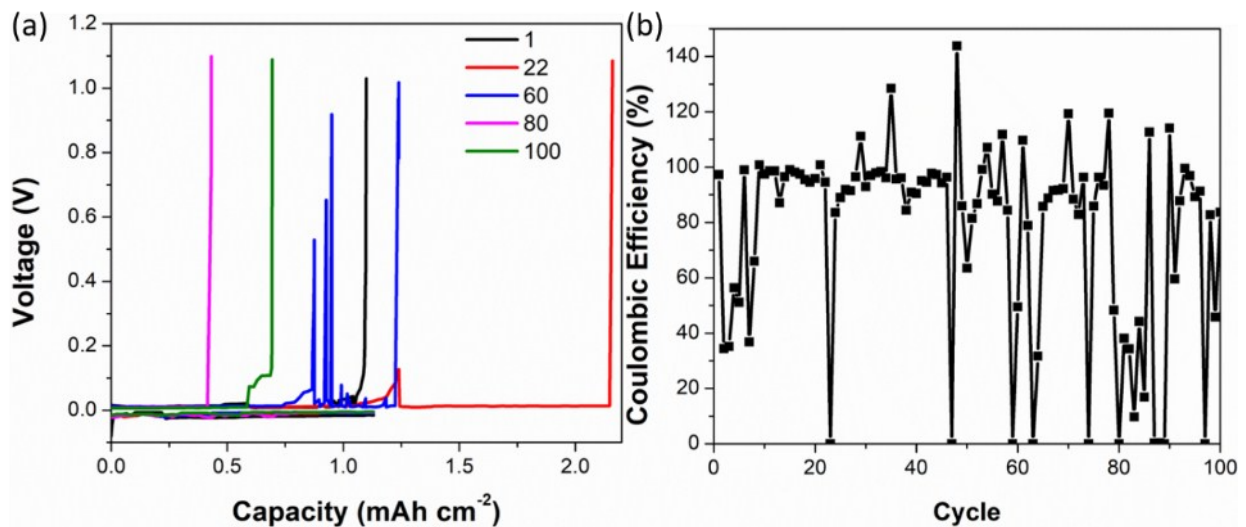
Fig. S16. (a) Half-cell voltage profiles; and (b) Coulombic efficiencies of Al foil current collector.
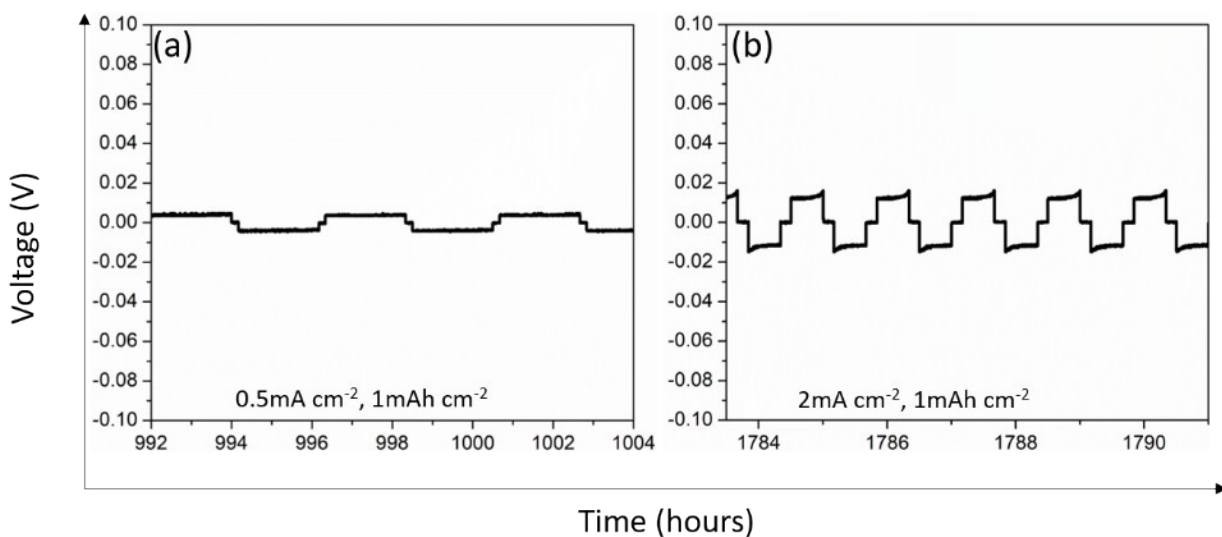
Fig. S17. Magnified views of voltage vs time curves of PCNF-700 symmetric cell at different cycle times and current densities: (a) at 0.5 mA cm^{-2} and 1 mAh cm^{-2}; and (b) at 2 mA cm^{-2} and 1 mAh cm^{-2}.
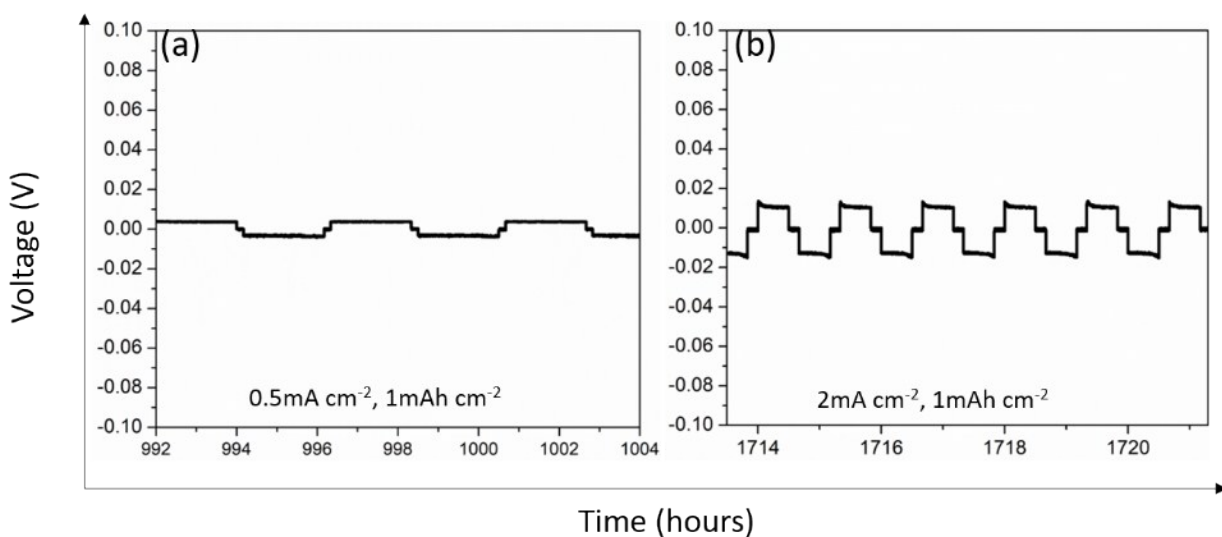
Fig. S18. Magnified views of voltage vs time curves of PCNF-800 symmetric cell at different cycle times and current densities: (a) at 0.5 mA cm^{-2} for 1 mAh cm^{-2}; and (b) at 2 mA cm^{-2} for 1 mAh cm^{-2}.
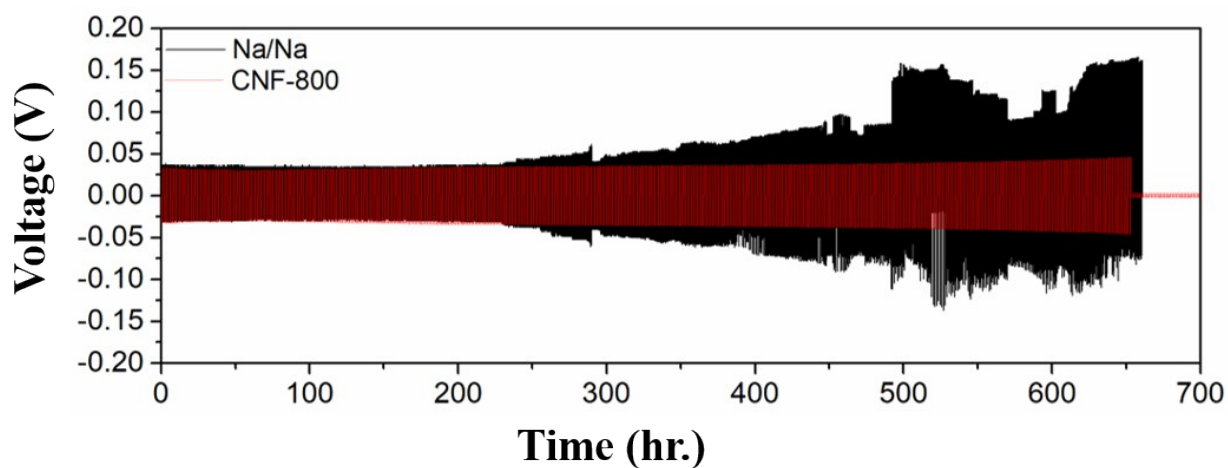
Fig. S19. Symmetric cell performance of Na/Na and CNF-800 electrode at 1mA cm^{-2} for a capacity of 1mAh cm^{-2}.
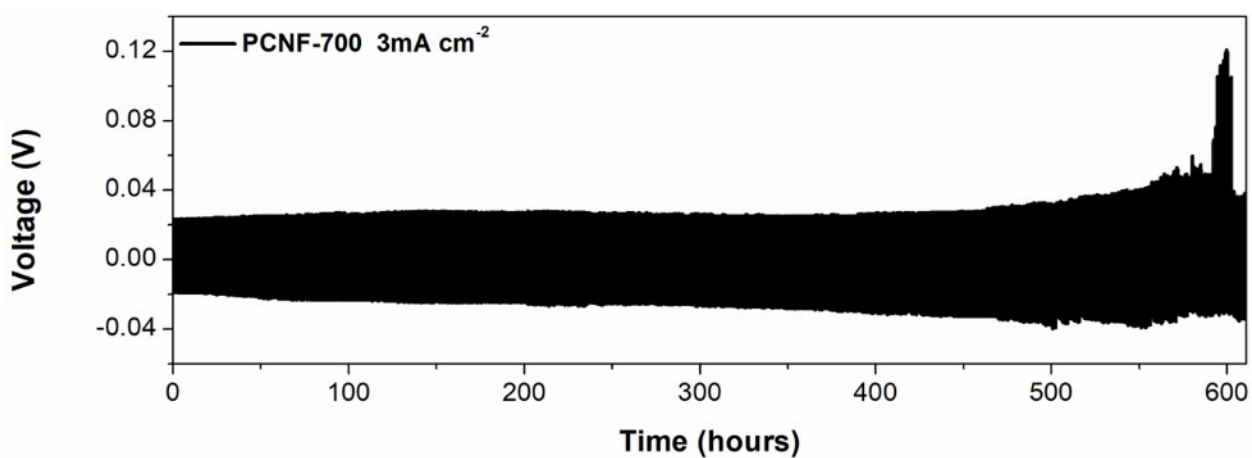
Fig. S20. Symmetric cell performance of the PCNF-700 electrode at a current density of 3mA cm^{-2} for a capacity of 1mAh cm^{-2}.
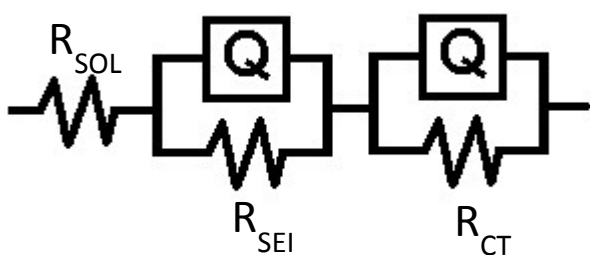
Fig. S21. Equivalent fitting circuit for EIS measured data.
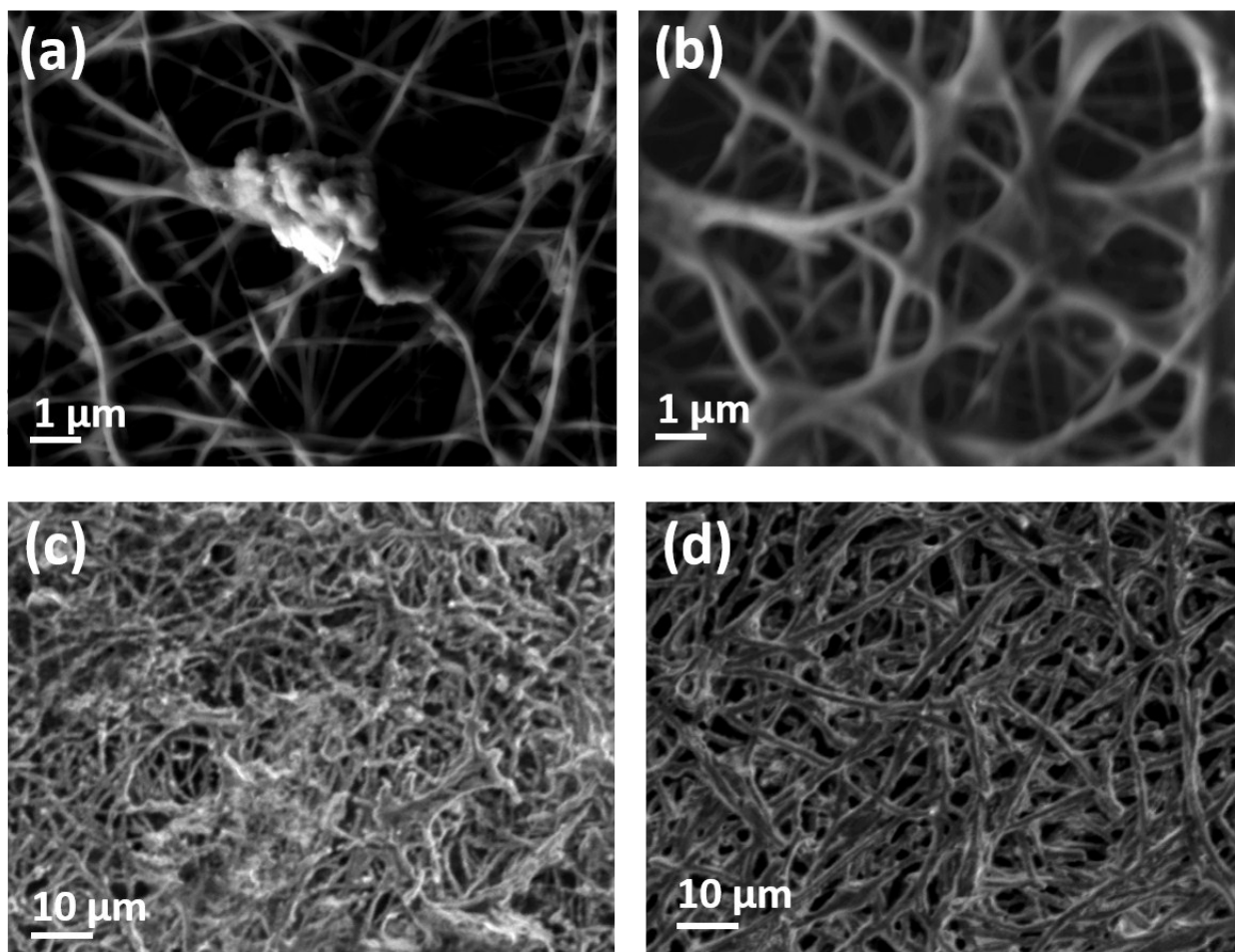
Fig. S22. Na plating behavior examined at a current density of 1 mA cm^{-2}. *Ex Situ* SEM images of (a) CNF-800 and (b) PCNF-800 hosts taken at the initial stage; and of (c) CNF-800 and (d) PCNF-800 hosts after plating of 0.3 mAh cm^{-2}.
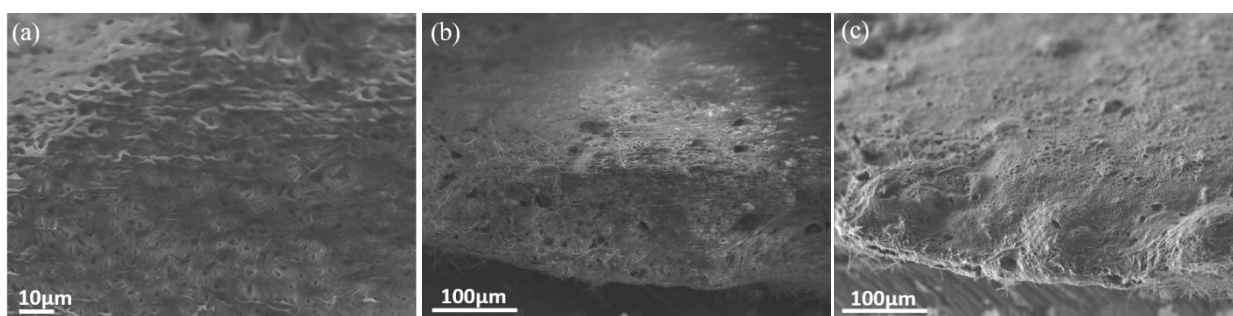
Fig. S23. *Ex-situ* cross-sectional SEM micrographs of the PCNF-800 electrodes tested at different current densities and areal capacities: (a) 2mA cm^{-2} for 2mAh cm^{-2}; (b) 3mA cm^{-2} for 3mAh cm^{-2}; and (c) 5mA cm^{-2} for 3 mAh cm^{-2}.
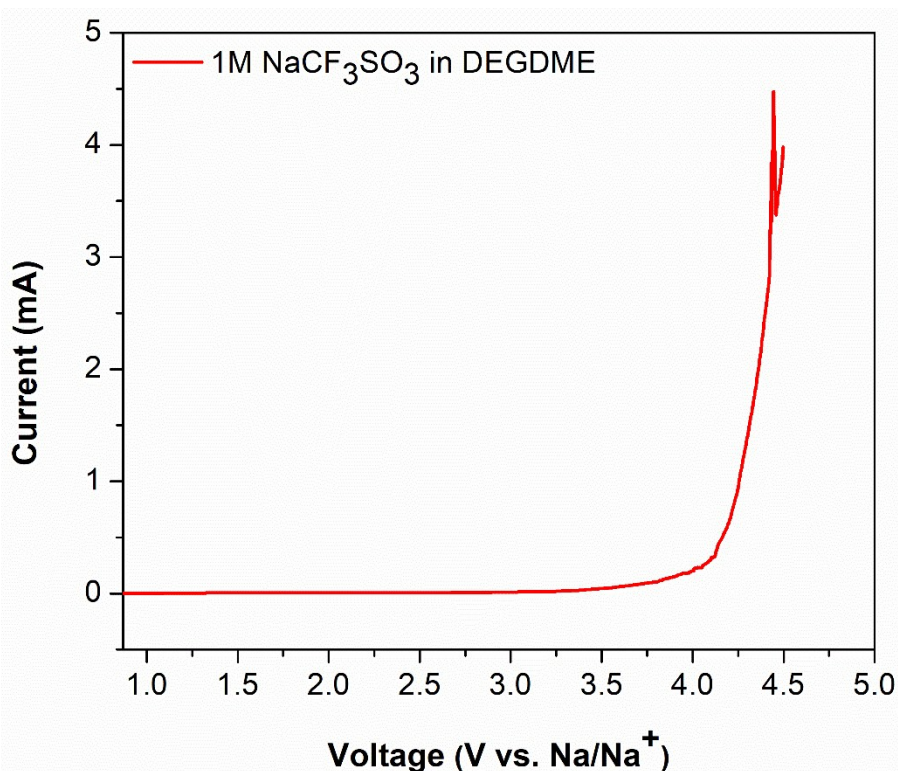
Fig S24. LSV curve that determines the electrochemical stability window of 1M $NaCF_3SO_3$ DEGDME electrolyte using SS as the working electrode and Na foil as reference and counter electrode at a scan rate of 0.5 mV/s.
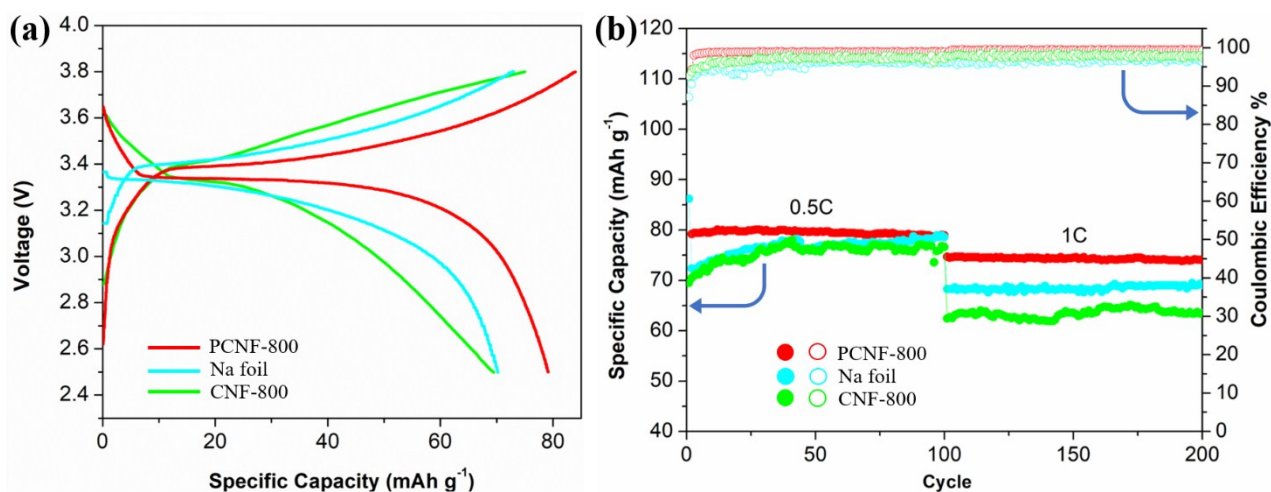
Fig S25. Electrochemical performance of full cells. (a) GCD profiles at 0.5 C, and (b) Cyclic performance at different current densities of full cells consisting of Na@PCNF-800/NVP, Na@CNF-800/NVP, or Na foil as the anode and NVP/C as the cathode.

Density Functional Theory (DFT) Calculations

The density functional theory (DFT) calculations were performed based on the first principles theory using Vienna *Ab-initio* Simulation Package (VASP) [S2] with a projected augmented wave approach. The exchange-correlation functional energy was processed by the Perdew-Burke-Ernzerhof (PBE)

function within the generalized gradient approximation (GGA). [S3, 4] The kinetic energy cutoff was set to 520 eV with the total energy converged to 10^{-5} eV. All optimized structures were obtained by fully relaxing atomic positions until the Hellmann−Feynman forces on all atoms were smaller than 0.02 eV/Å. For the relaxation of multilayer carbon structure, a 2×3 in-plane supercell was adopted with representative AB stacking three layers to accurately describe the interlayer C-C interaction. [S5] The bottom carbon layer was fixed, representing the artificial multilayer of the carbon structure. The Brilliouin zone was represented by a gamma-centered k-point grid of 5×5×1. To avoid the periodic image interaction between the two nearest neighbor unit cells, the vacuum was set to 40 Å in the *c*-axis. The whole multilayer structure optimization was carried out by considering the van der Waals corrected density functional theory (DFT-DF2) proposed by Langreth and Lundqvist et al. [S6] to overcome the deficiencies of DFT in treating dispersion interactions between the interlayer atoms. The adsorption energy of a Na single atom on the surface of multi-layer carbon structure was obtained from Equation (S1).

$$E_{ad} = E_{NHG + Na} - E_{NHG} - \mu_{Na} \tag{S1}$$

where $E_{NHG + Na}$ and E_{NHG} are the total energies of multi-layer carbon structure with and without Na adatom, and μ_{Na} is the energy of Na leveled from the atomic state. The adsorption sites of single Na atom are optimally selected on all multilayer carbon structure with a defect in proximity to the functional groups. The charge transfer between the Na atom and multi-layer carbon structure was evaluated by Equation (S2)

$$\Delta\rho = \rho_{NHG + Na} - \rho_{NHG} - \rho_{Na} \tag{S2}$$

where $\rho_{NHG + Na}$, ρ_{NHG} and ρ_{Na} are the charge densities of Na-adsorbed structures, multi-layer carbon, and isolated Na atom, respectively. The structures were visualized and plotted using Vesta software. [S7]
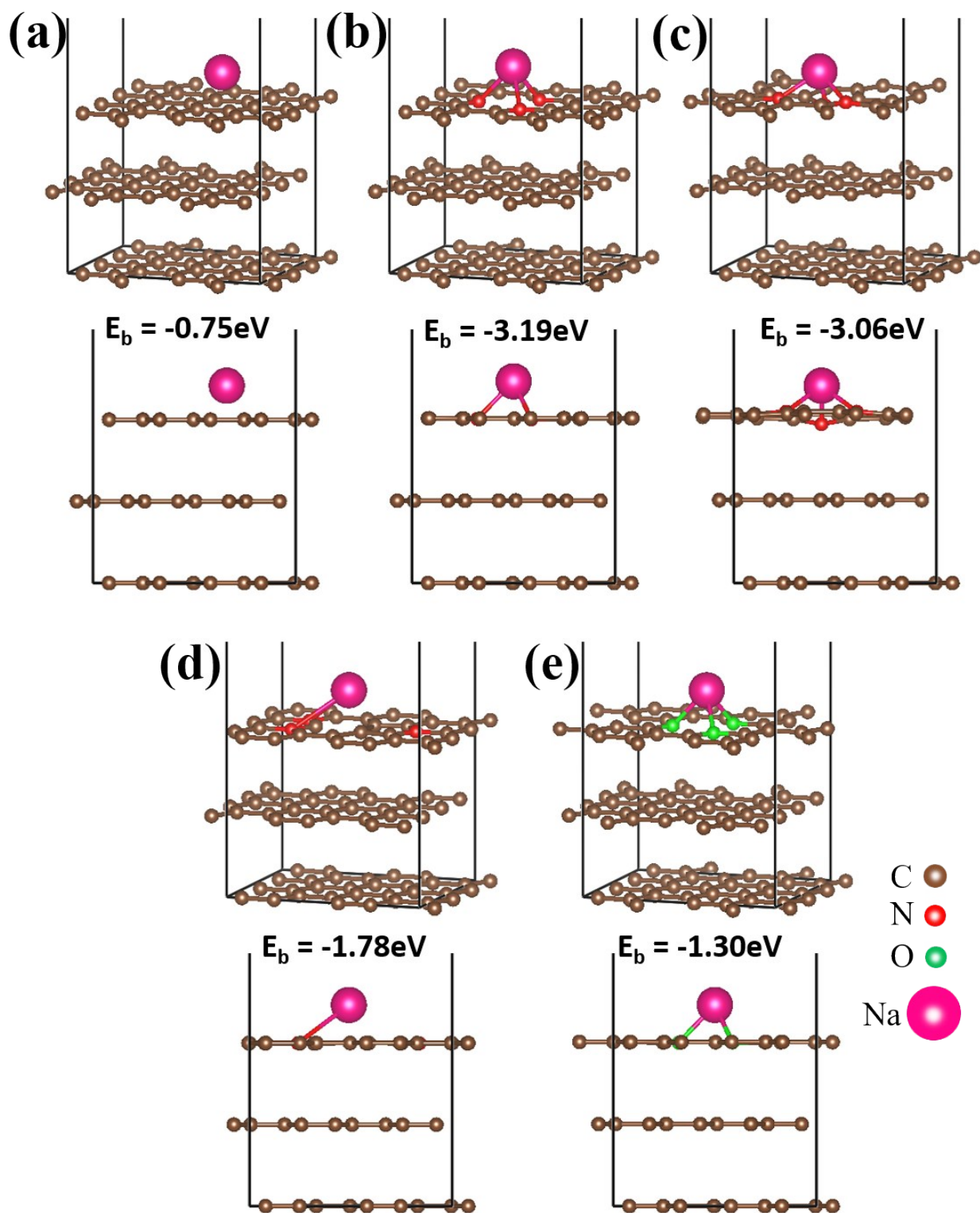
Fig. S26. Optimized structures of multilayer carbon system after relaxation. Standard orientation and side views (a) defect-free graphite, (b) pyridinic-N (c) pyrrolic-N (d) graphitic-N (e) carbonyl groups on defective carbon structure.
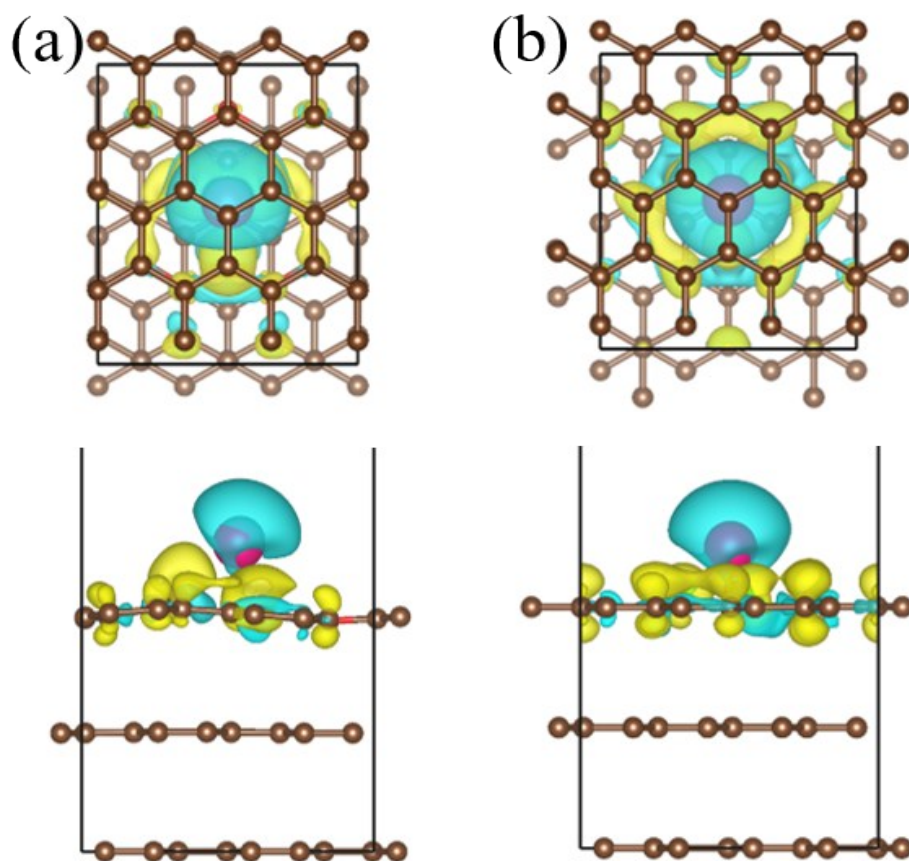
Fig. S27. Charge density difference plots of (a) graphitic-N (G-N) (b) carbonyl group (=CO) on defective carbon structure.

(a)

$E_b = -3.19$ eV

(b)

$E_b = -3.15$ eV
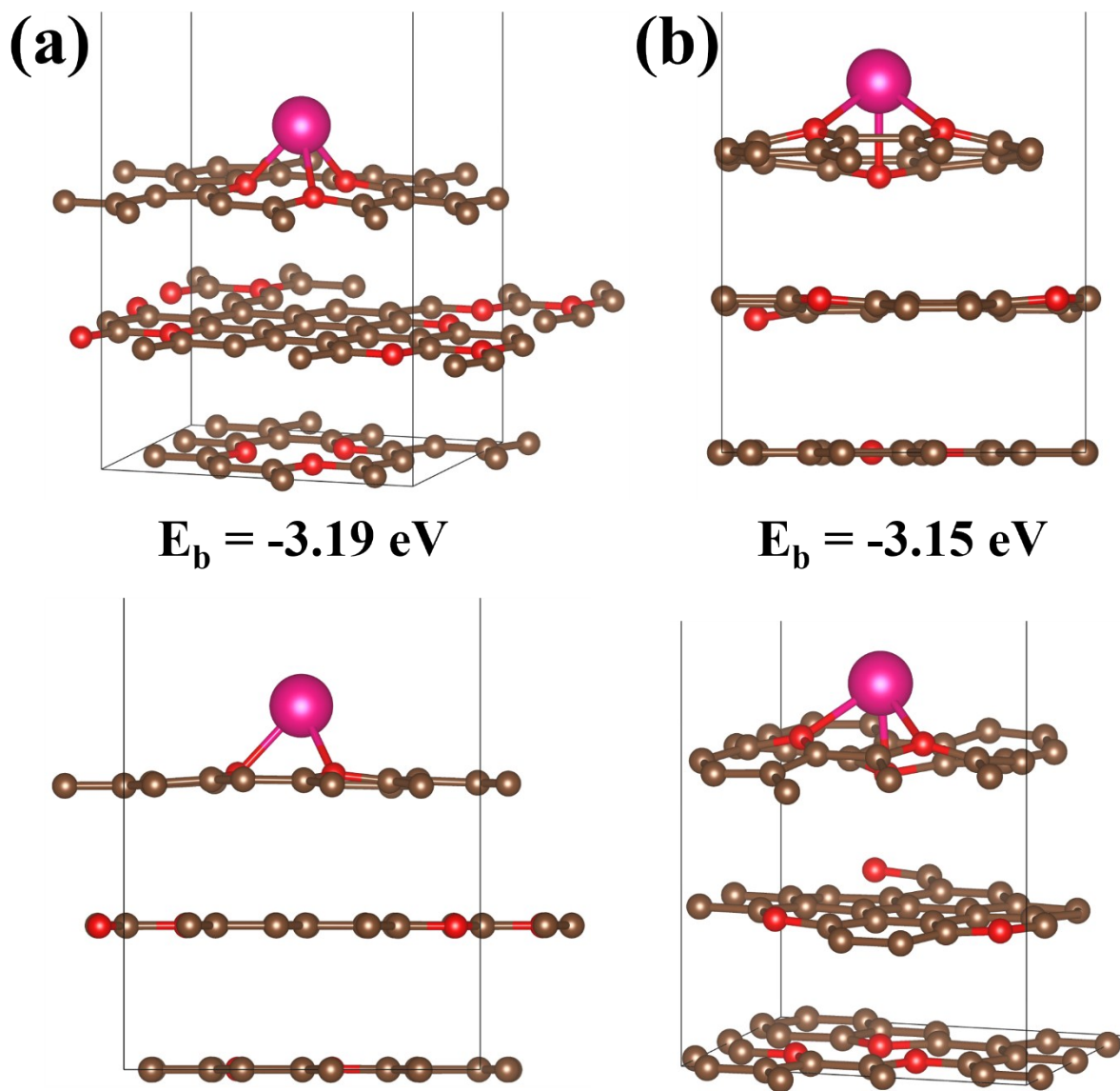
Fig S28. Optimized structures of multilayer carbon system with extensive defects and functional groups after relaxation. Standard orientation and side views (a) pyridinic-N and (b) pyrrolic-N groups in all carbon layers
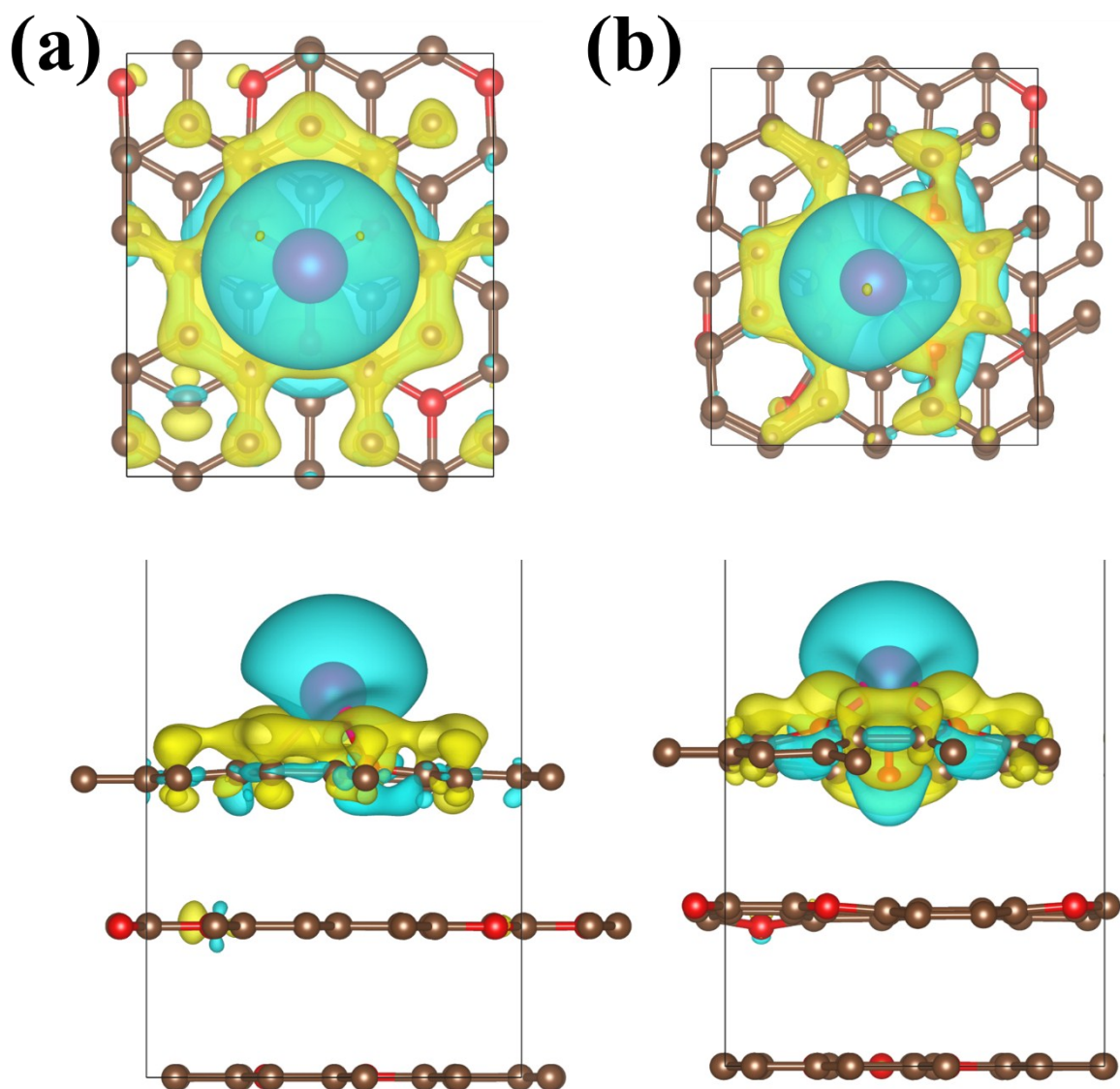
Fig S29. Charge density difference plots with extensive defects and functional groups (a) pyridinic-N and (b) pyrrolic-N in all carbon layers.

Fig. S30. Photographic snapshots of multiple PCNF-800 electrodes indicating successful melt infiltration of Na. Scale bar = 10 mm.
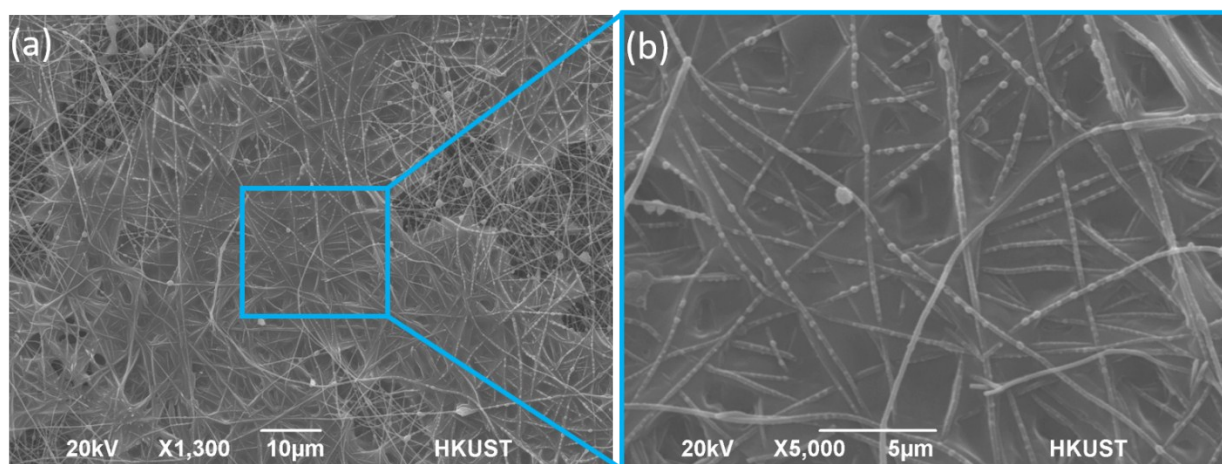
Fig. S31. SEM micrographs showing uniform Na infusion through the entire carbon structure.

The electronic conductivities increased with increasing carbonization temperature, also aided by the catalytic graphitization of Ni nanoparticles that created highly conductive, ordered short-range domains around them. This is evident from the highest conductivity of 2.84 S/cm achieved by the PCNF electrode carbonized at 1,000°C among different CNFs (Table S1).

Table S1. BET surface areas, pore volumes and electrical conductivities of neat CNFs and PCNFs.

Materials	Surface Area [m^2/ g^{-1}]	Pore Volume [$cm^3 g^{-1}$]	Electrical Conductivity [$S cm^{-1}$]
CNF-800°C	10.9	0.095	0.90
PCNF-700°C	129.6	0.194	0.86
PCNF-800°C	187.3	0.351	1.21
PCNF-1000°C	210.8	0.335	2.84

Table S2. Elemental compositions and percentage of individual functional groups for neat CNFs and PCNFs.

Materials [At. conc. %] [%]	C				O		N				Zn
	C-C	C=C	C=O	C-C=O	C-OH	C=O	Pr-N	Py-N	G-N	O-N	
CNF-800	**88.8**				**1.7**		**9.5**				-
	53	34	5	8	77	23	33	48	8	11	
PCNF-700	**80.3**				**3.2**		**14.7**				**1.8**
	45	34	9	12	75	25	49	27	16	8	
PCNF-800	**84.6**				**4.5**		**9.8**				**1.1**
	48	28	12	12	72	28	42	42	4	12	
PCNF-1000	**93.0**				**2.9**		**4.1**				-
	57	21	8	14	78	22	35	36	15	14	

Pr-N, Py-N, G-N and O-N are Pyridinic-N, Pyrrolic-N, Graphitic-N and Oxidized-N functional groups respectively.

Table S3. Impedance parameters obtained from EIS Nyquist spectra of the PCNF-800 electrode.

Time (hr]	0	10	100	300	500	700	1000
R_{SOL} (Ω]	2.22	2.39	2.38	2.62	2.64	2.63	2.66
R_{SEI} (Ω]	5.77	2.72	2.34	0.96	1.24	1.20	1.32
R_{CT} (Ω)	5.42	1.99	1.27	2.13	2.39	1.86	2.11

Table S4. Comparison of electrochemical performance between the current PCNF Na metal batteries and those prepared from state-of-the-art modified carbonaceous materials.

Materials [Ref.]	Current density (mA cm^{-2})	Areal capacity (mA h cm^{-2})	Cycle number/hour	Coulombic efficiency (%)	Electrolyte
Defect-engineered electrospun PCNF-800 **(Current Work)**	**1**	**1**	**600 cycles**	**99.8%**	**NaSO$_3$CF$_3$ (1M) in DEGDME**
	0.5	**1**	**1500 h**		
	1	**1**	**4000 h**		
	2	**1**	**500 h**		
	3	**1**	**2000 h**		
CNTs* with oxygenic groups [39]	0.5	1	1000 cycles	99.8%	NaSO$_3$CF$_3$ (1 M) in DEGDME
	1	1	1600 cycles	99.9%	
	3	1	1000 cycles	99.8%	
	1	1	250 h		
	3	1	1100 h		
	3	3	320 h		
	5	8	310 h		
Conductive carbon black [43]	0.5	0.25	>1000 cycles	99.8%	NaPF$_6$ (1 M) in DEGDME
	1	12	>50 cycles	99.9%	
Na@rGO composite [48]	1	1	600 h		NaPF$_6$ (1 M) in DEGDME
	0.25	0.08	300 h		NaSO$_3$CF$_3$ (1 M) in DEGDME
	3	3	300 h		NaSO$_3$CF$_3$ (1 M) in DEGDME
	5	5	300 h		NaSO$_3$CF$_3$ (1 M) in DEGDME
	0.25	0.06	300 h		NaClO4 (1 M) in EC/PC
	0.5	0.125	60 h		NaClO4 (1 M) in EC/PC
Na-carbonized wood [25]	1	0.5	250 h		NaClO$_4$ (1 M) in EC: DEC
	1	1	500 h		
Graphitized carbon microspheres/Na [44]	1		175 cycles	98.9%	NaPF$_6$ (1 M) in DEGDME
	0.5	1	3600 h		
3D flexible carbon	1	2	120 cycles		NaClO$_4$ (1 M) in

felt/Na [31]					EC/PC
	3	2	120 cycles		NaClO$_4$ (1 M) in EC/PC
	5	2	120 cycles		NaClO$_4$ (1 M) in EC/PC
	3	3	200 cycles		NaTFSI (1 M) in DOL/DME
Macroporous catalytic carbon nanotemplate [41]	1	0.5	1200 cycles	99.9%	NaPF$_6$ (1 M) in DEGDME
Sodium infiltrated Fe$_2$O$_3$ coated carbon textile [46]	1	1	333 h		NaClO$_4$ (1 M) in EC: DMC
	3	1	222 h		
	5	1	138 h		
Carbon paper with N-doped CNT*/Na [42]	1	1	350 h		NaPF$_6$ (1 M) in EC:PC
	3	1	180 h		
	5	1	140 h		
	5	3	90 h		
N, S co-doped CNT* paper [47]	1	1	500 h		NaSO$_3$CF$_3$ (1 M) in DEGDME
	3	1	150 h		
	1	1	400 cycles	99.82%	
	2	1	500 cycles	99.87%	
	1	5	200 cycles	99.79%	
N, O co-doped graphitized carbon fibers [38]	1	8	~100 cycles	99.9%	NaPF$_6$ (1 M) in DEGDME
	2	8	>120 cycles	99.8%	
	0.5	1	800 h		
	1	1	1260 h		
Ultrathin graphene films [45]	0.5	0.5	200 h		NaPF$_6$ (1 M) in EC:DEC
	0.25	1	60 h		
	1	1	200 h		
	2	1	125 h		
	2	3	300 h		
Carbon paper pressed onto Na [40]	1	1	200 cycles		NaClO$_4$ (1 M) in PC with 5 vol% FEC
	0.5	1	250 cycles		NaSO$_3$CF$_3$ (1 M) in DEGDME
	5	1	1200 cycles		NaSO$_3$CF$_3$ (1 M)

					in DEGDME

*CNT = carbon nanotube

Supplementary Videos V1: The video shows real-time melt infiltration of Na into the PCNF-800 electrode.

References

S1   C. Kim, S.-H. Park, J.-I. Cho, D.-Y. Lee, T.-J. Park, W.-J. Lee, K.-S. Yang, *J. Raman Spectrosc.,* 2004, **35**, 928.
S2   G. Kresse, J. Furthmuller, *Phys. Rev. B,* 1996, **54**, 11169.
S3   M. Ernzerhof, G.E. Scuseria, *J. Chem. Phys.,* 1999, **110(11)**, 5029.
S4   B. Hammer, L.B. Hansen, J.K. Norskov, *Phys. Rev. B,* 1999, **59(11)**, 7413.
S5   H. Huang, H.-H. Wu, C. Chi, J. Zhu, B. Huang, T.-Y.J.N. Zhang, *Nanoscale,* 2019, **11(40)**, 18758.
S6   K. Lee, E.D. Murray, L.Z. Kong, B.I. Lundqvist, D.C. Langreth, *Phys. Rev. B,* 2010, **82(8)**.
S7   K. Momma, F. Izumi, *J. Appl. Crysallogr.,* 2011, **44**, 1272.